Noisy FitzHugh-Nagumo model: From single elements to globally coupled networks

J. A. Acebrón,[1] A. R. Bulsara,[2] and W.-J. Rappel[1]

[1]*Department of Physics, University of California, San Diego, La Jolla, California 92093, USA*
[2]*SPAWAR Systems Center Code D363, 49590 Lassing Road, RM A341 San Diego, California 92152-6147, USA*

We study the noisy FitzHugh-Nagumo model, representative of the dynamics of excitable neural elements, and derive a Fokker-Planck equation for both a single element and for a network of globally coupled elements. We introduce an efficient way to numerically solve this Fokker-Planck equation, especially for large noise levels. We show that, contrary to the single element, the network can undergo a Hopf bifurcation as the coupling strength is increased. Furthermore, we show that an external sinusoidal driving force leads to a classical resonance when its frequency matches the underlying system frequency. This resonance is also investigated analytically by exploiting the different time scales in the problem.

I. INTRODUCTION

The response of dynamical systems to noise has long been an active field of study, mostly driven by its enormous relevance in numerous applications in engineering, physics, biology, and medicine. In this context, noisy dynamical systems also present the researcher with interesting physical and mathematical problems which have led to the development of a number of analytical and numerical techniques. Often, noise is an undesirable element of the dynamical system and considerable previous work has focused on techniques that can suppress its effects in real applications. However, not all noise is bad; indeed, sometimes the system "tunes" itself to achieve optimal response as a function of a given noise floor. This has led to extensive investigations of noise-mediated cooperative behavior, e.g., stochastic resonance [1], and noise-enhanced propagation [2], as well as more rigorous investigations into the behavior of bifurcating dynamical systems in the presence of noise [3]; in essence one develops a strategy that, instead of minimizing the noise, searches for the area in the system parameter space wherein the optimal response in the presence of a given noise floor is obtained. This is particularly relevant in the context of neural dynamics, it being generally accepted that neurons adjust their dynamical parameters (e.g., firing thresholds) to achieve optimal information throughput, in the presence of noise [4]; as suggested here, the response to more complex signals must be characterized by measures that are somewhat more general than simply an output signal-to-noise ratio. An additional improvement in the response can often be obtained when the number of elements is increased. This, then, leads to a study of noisy nonlinear dynamics in coupled systems and a wide variety of coupling schemes have been studied [5]. A systematic investigation of networks, however, can be computationally costly since it requires solving numerous coupled stochastic differential equations.

In this paper, we investigate the effect of noise in the FitzHugh-Nagumo model (FHN) [6,7] which has become a popular representation of dynamical systems for several reasons. First, its relative simple structure sometimes allows one to make analytical progress. Second, by varying the parameters, the FHN admits a number of standard dynamics including periodic oscillations, stable fixed points, and excitability. Third, the FHN has been used as a simple model for both neurons [8] and cardiac tissue [9], making it relevant to biomedical systems.

Our main approach consists of the recasting of the noisy FHN equations into the Fokker-Planck equation (FPE). We will do this for both the single element and for a system of globally coupled elements. In the latter case, the FPE approach allows us to investigate the coupled system in a computationally efficient fashion. In addition, we will include a probe signal, taken to be a time-sinusoidal driving term. Particular attention is paid to the *deterministic* resonance effects that can arise when a system with an underlying frequency is subject to this probe signal [10]. In recent work [11], we have studied such resonance behavior for a noisy two-dimensional (2D) system (the two-junction superconducting quantum interference device or dc SQUID), which follows somewhat different dynamics (the bifurcation phenomena are different) than the FHN model considered in this work; our results have shown that frequency information about an external "target" signal may be extracted by sweeping the system control parameters until the characteristic (internal) frequency matches the external signal frequency, a direct exploitation of the deterministic resonance behavior that such systems demonstrate, even in the presence of a noise floor.

The paper is organized as follows: in the following section, we introduce our model and derive the FPE. We then examine our results for a single element and discuss their connection with recently published work. In Sec. III we study a network of globally coupled FHN elements with, and without, a probe signal. Finally, we conclude with a discussion of our results.

II. SINGLE ELEMENT

The FHN is a simplified version of the well-known Hodgkin-Huxley model [12], which describes the firing mechanism in an excitable nerve cell. In the FHN, the dynamics of the nerve cell are reduced to two variables: a fast activation variable, corresponding to the voltage, and a slow recovery variable [13]. This reduction allows one to visualize

the dynamics by drawing the nullclines (the lines corresponding to the steady states of the two variables) in phase space. As mentioned before, the FHN displays a rich phase diagram that includes excitable, oscillatory, and bistable regimes, rendering it suitable for use a model system in the field of pattern formation (see, e.g., Ref. [14]). The inclusion of noise has been investigated for both single FHN elements (see, e.g., Refs. [15,16]) and populations of coupled FHN elements (see, e.g., Ref. [18]). In addition, the periodically driven FHN, where either the slow or the fast equation contains a time-periodic driving term, has received considerable attention [19].

Let us start with the most general form of the FHN system:

$$\frac{dx}{dt} = Ax^3 + Bx^2 + Cx + Hy + I + \xi,$$

$$\frac{dy}{dt} = Ex + Fy + G. \tag{1}$$

Here, $x(t)$ is the voltage variable, $y(t)$ is the recovery variable, and I represents an external stimulus. Furthermore, ξ is a Gaussian noise source having zero mean, and correlation function $\langle \xi(t)\xi(t') \rangle = 2D\delta(t-t')$ and A through G are parameters that govern the dynamics of the system. To make the treatment in this paper as general as possible, all relevant analytical expressions will be derived using the above set of equations. However, when presenting results of numerical calculations, we have chosen to limit ourselves to the investigation of the FHN in one of its more conventional representations

$$\frac{dx}{dt} = \frac{x(x-a)(1-x)-y}{\alpha} + \xi,$$

$$\frac{dy}{dt} = x - py - b. \tag{2}$$

where α, a parameter measuring the separation of time scales, is typically taken to be small. Conversion between Eqs. (1) and (2) is straightforward.

A. The single-element Fokker-Planck equation (FPE)

As promised above, we will study the noisy FHN model, via the FPE approach. This approach is motivated by the fact that for parameters values for which analytical progress is difficult to achieve one has to resort to numerics. In this case, direct simulation of the Langevin equations (1), as has been commonly done in the FHN repertoire, can be computationally intensive: for reasonably accurate results one typically has to average over many runs, particularly for systems close to a bifurcation point where one must distinguish between different stable solutions, and for large-noise scenarios. Numerical solutions of the FPE, on the other hand, can be obtained much faster.

The FPE for the single-element FHN is readily written down using standard methods [20]

$$\frac{\partial \rho}{\partial t} = D\frac{\partial^2 \rho}{\partial x^2} - \frac{\partial}{\partial x}[(Ax^3 + Bx^2 + Cx + Hy + I)\rho]$$

$$- \frac{\partial}{\partial y}[(Ex + Fy + G)\rho], \tag{3}$$

where $\rho(x,y)$ is the probability density function. As usual, the FPE has to be accompanied by initial and boundary data (decay to zero as $x \to \pm\infty, y \to \pm\infty$, with sufficiently high rate), and the normalization condition

$$\int_{-\infty}^{+\infty}\int_{-\infty}^{+\infty} dxdy\rho(x,y,t) = 1. \tag{4}$$

It turns out that our FPE has a unique stationary solution, which can be seen by observing that there exists a Lyapunov function (see Ref. [20] and references therein). The existence of the Lyapunov function guarantees that the stationary solution is unique and globally stable.

To ensure numerical efficiency we have chosen not to solve the FPE via a finite difference [21] or finite element scheme [22]. Rather, we have used a spectral method in which we expand the probability density ρ using a basis of Hermite polynomials [23]:

$$\rho(x,y,t) = \sum_{n=0}^{\infty}\sum_{m=0}^{\infty} r_n^m(t)H_n(x)H_m(y)e^{-x^2}e^{-y^2}. \tag{5}$$

Note that this expansion satisfies the boundary conditions, and the normalization condition with $r_0^0 = 1/\pi$. After inserting Eq. (5) into the FPE (3) we obtain the following hierarchy of coupled ordinary differential equations for $r_n^m(t)$:

$$\dot{r}_n^m = (\tfrac{3}{2}An^2 + Cn + Fm)r_n^m + [B(n-1)+I]r_{n-1}^m$$

$$+ [D + \tfrac{3}{4}A(n-1) + \tfrac{1}{2}C]r_{n-2}^m + \frac{B}{4}r_{n-3}^m + \frac{A}{8}r_{n-4}^m$$

$$+ Bn(n+1)r_{n+1}^m + An(n+1)(n+2)r_{n+2}^m + Gr_n^{m-1}$$

$$+ \frac{F}{2}r_n^{m-2} + \tfrac{1}{2}(H+E)r_{n-1}^{m-1} + E(n+1)r_{n+1}^{m-1}$$

$$+ H(m+1)r_{n-1}^{m+1},$$

$$\text{where} \quad n = 0,1\dots,\infty, m = 0,1,\dots,\infty, \tag{6}$$

with $\bar{x}$ and $\bar{y}$

$$\bar{x} = \int_{-\infty}^{+\infty}\int_{-\infty}^{+\infty} dxdyx\rho(x,y,t) = \pi r_1^0, \tag{7}$$

$$\bar{y} = \int_{-\infty}^{+\infty}\int_{-\infty}^{+\infty} dxdyy\rho(x,y,t) = \pi r_0^1. \tag{8}$$

This infinite hierarchy is then truncated at $n=N$ and $m=M$, setting $r_{N+1}^{M+1}=0$.

Our numerical scheme is particularly efficient for large noise levels, where a small number of coefficients is already
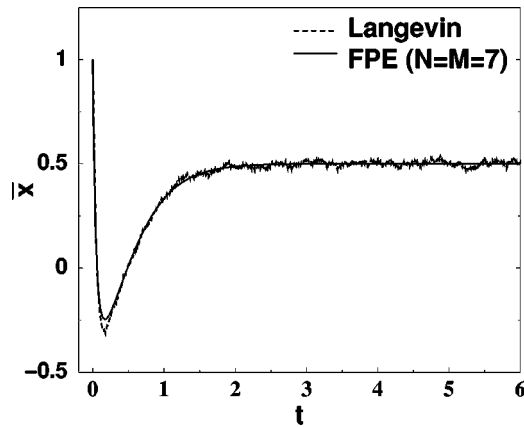
FIG. 1. Comparison between the numerical solution of the Langevin equations (2) (averaged over 500 realizations) and the solution of the Fokker-Planck equation by the spectral method with $N=M=7$ coefficients. Parameters are $D=8$, $b=0.5$, $p=1$, $\alpha=0.05$, $a=0.5$, for which the deterministic system is oscillatory.

sufficient to give excellent numerical answers. This can be seen in Fig. 1, where we plot the first moment $\bar{x}$ as a function of time, obtained numerically by solving the Langevin equations (1) and averaging over a large number of realizations, and by solving the FPE using the above-described spectral method. The spectral method (with $N=M=7$ coefficients) is seen to provide excellent agreement with the more conventional and time-consuming technique based on numerically integrating the coupled stochastic differential equations (1).

Once a suitable algorithm is implemented to solve the FPE it is straightforward to find the probability density function corresponding to its unique stationary solution [22]. In Fig. 2 we have plotted the marginal density $\rho_x(x) = \int_{-\infty}^{+\infty} dy \rho(x,y)$ for two different noise levels calculated using the FPE (solid lines) and via Langevin simulations (dashed lines). Again, the agreement between the Langevin simula-
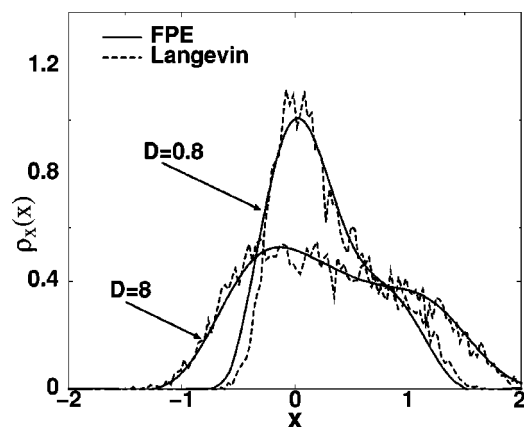

FIG. 2. Marginal density $\int_{-\infty}^{+\infty} dy \rho(x,y)$ obtained through the numerical solution of the Langevin equations (2) (averaged over 500 realizations) and the solution of the Fokker-Planck equation by the spectral method with $N=M=7$ coefficients when $D=8$, and $N=M=30$ coefficients when $D=0.8$. Parameters are $b=0.2$, $p=1$, $\alpha=0.05$, and $a=0.5$, for which the deterministic system is excitatory.

tions and the numerical solutions of the FPE using our algorithm is excellent. For the smaller noise level, $\rho_x(x)$ becomes more peaked around the fixed point and more coefficients need to be taken into account: $N=M=30$ vs $N=M=7$ for the higher noise level.

B. "Stochastic bifurcation:" A brief digression

Contrary to deterministic systems, the definition of a bifurcation in stochastic systems is not very precise. One previously employed way of defining phenomenological stochastic bifurcations is to focus on a qualitative change in a time-averaged quantity [3]. Examples of this can be a probability density function or powerspectrum, which undergoes a qualitative change from single peaked to double peaked [24].

Recently, several studies have attempted to address the issue of stochastic bifurcations in the FHN [16]. Tanabe and Pakdaman extended and refined the treatment by Rodriguez and Tuckwell and found expressions for the mean, variance, and covariance of the dynamical state variables in the FHN [17]. These expressions were derived by assuming the distribution of the variables to be Gaussian. Tanabe and Pakdaman first demonstrated that, using Langevin simulations of the full dynamics, the steady state distributions of the variables could undergo a qualitative transition from unimodal, for small values of the noise intensity, to bimodal for larger values of the noise. They used the equations for the moments to obtain a bifurcation diagram in noise vs system parameter space. They found that the first moment of the fast variable undergoes a Hopf bifurcation at a critical value of the current intensity I which approached the critical value for the deterministic Hopf bifurcation as the noise level was decreased. They then concluded that one could define a stochastic bifurcation in the FHN that was an extension of the deterministic one.

It is important to note that the occurrence of a second peak in the probability distribution corresponds to the occasional escape of an element from its fixed point. Upon increasing the strength of the noise, the probability of escape becomes larger and such a peak becomes more pronounced. However, even for very small noise levels, the state point has a nonzero probability to escape from the fixed point, leading to a small but nonzero second peak in the probability distribution. Thus, defining a stochastic bifurcation based on the occurrence of a second peak is problematic.

In addition, caution needs to be exercised when linking the "bifurcation" in the moment equations to a stochastic bifurcation. As we have mentioned before, the FPE is linear and has unique, stationary, and globally stable solutions. Consequently, the moments of the FHN cannot exhibit a Hopf bifurcation. The Hopf bifurcation found in Ref. [17] is, most likely, an artifact of the limited number of moments considered; one would expect that increasing the number of moments, an admittedly very difficult and cumbersome task, will lead to the disappearance of the Hopf bifurcation.

From the above, we conclude that we cannot provide a meaningful definition of a stochastic bifurcation in a single FHN element. However, as we will see below, the globally
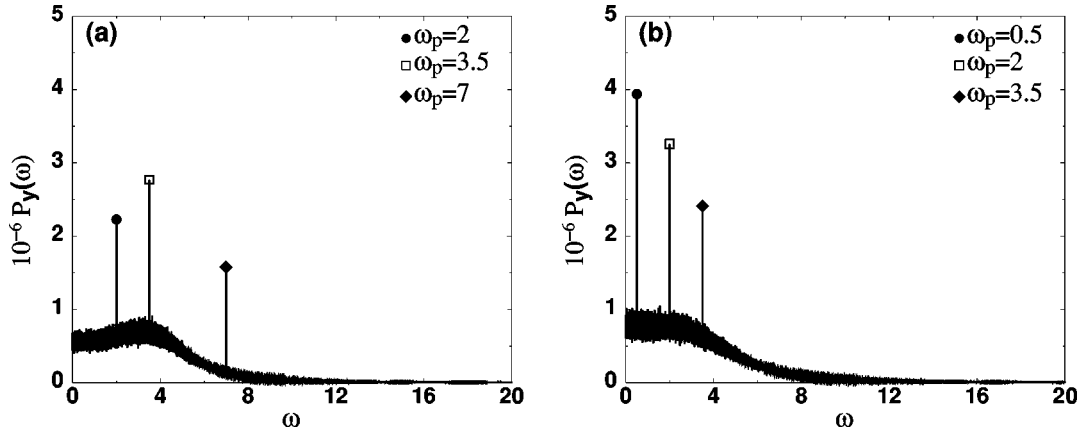
FIG. 3. Power spectrum of the variable y for three different values of the probe signal, and noise strength; (a) $D=1.2$, and (b) $D=2$. Simulations done by using the Langevin equations. Other parameters are $b_0=0.5$, $p=1$, $q=0.01$, $\alpha=0.05$, and $a=0.5$

coupled case *does* exhibit a true stochastic Hopf bifurcation, related to the synchronization of the network. Also, as we will discuss in the following section, even without determining the location of a stochastic bifurcation, we can still find the underlying (or characteristic) frequency of the noisy single FHN element.

C. Inclusion of a probe signal

We now turn to the inclusion of a probe signal by considering a sinusoidal external component in Eqs. (1) and (2) via $G=G_0+q\sin(\omega_p t)$ and $b=b_0+q\sin(\omega_p t)$, respectively. The motivation stems from the desire, in many systems it is desirable to obtain the internal (or natural) frequency of the system. Our recent work [11] has already demonstrated the utility of determining this frequency (in terms of laboratory-controllable system parameters), as a means towards optimal performance (in the presence of a noise floor), as well as detection of an unknown "target" signal containing frequency information. The "resonance" in the output signal-to-noise ratio, exhibits some hallmarks of the well-studied stochastic resonance effect [1], however, since it occurs at a *deterministic* value of a system control parameter, precisely at the matching of the probe frequency with the (deterministic) internal oscillation frequency past the onset of a saddle-node bifurcation.

One way of determining this internal frequency is to compute $\bar{x}(t)$ or $\bar{y}(t)$ from the Langevin equations as time-dependent quantities; unfortunately, this is computationally very costly. On the other hand, aside from transients, $\bar{x}$ or $\bar{y}$ calculated from the FPE (which offers a computationally superior way to characterize the system), do not display a time-dependent behavior for a single FHN oscillator. Hence, we turn to the time-sinusoidal "probe" signal and the deterministic resonance that it sets up, to determine the internal frequency.

To illustrate the effect of the probe signal, we first performed Langevin simulations and calculated $\bar{y}$. In Fig. 3 we plot the power spectrum of this quantity for three different probe signals; two of them with frequencies ω_p that differ significantly from, and one that is very close to the underlying frequency. The power spectrum was obtained by averag-

ing 100 time series of 2^{23} time steps each. The figure illustrates clearly that, for a probe signal frequency that matches the broad peak corresponding to the (in general, nonsinusoidal) internal oscillations in the power spectrum of the unprobed system, the signal is amplified. Thus, adding the probe signal gives us a tool to investigate the dynamics of the noisy system and, specifically, to determine the intrinsic frequency of the system.

Even though it is in general much faster than directly simulating the driven Langevin equations, solving the time-dependent FPE can still be time consuming. Fortunately, we can reduce the time-dependent problem to a stationary one if we consider a small amplitude signal, $q=\varepsilon Q$, where $\varepsilon\ll1$. In this case, Eq. (3) contains terms with two different time scales thereby rendering the resulting FPE can be susceptible to analysis via the method of multiple scales; in turn we expect to be able to capture the long-time behavior of the probability density ρ.

The analysis begins by introducing fast and slow time scales as follows:

$$\tau=\frac{t}{\varepsilon}, \quad t=t. \tag{9}$$

We look for a distribution function satisfying the boundary condition according to the ansatz:

$$\rho(x,y,t;\varepsilon)=\sum_{n=0}^{2}\rho^{(n)}(x,y,t,\tau)\varepsilon^n+O(\varepsilon^3). \tag{10}$$

From Eq. (10), the average of x is given by

$$\langle x\rangle=\langle x\rangle^{(0)}+\varepsilon\langle x\rangle^{(1)}+O(\varepsilon^2), \tag{11}$$

where

$$\langle x\rangle^{(j)}=\int_{-\infty}^{+\infty}\int_{-\infty}^{+\infty}dxdyx\rho^{(j)}(x,y,t). \tag{12}$$

The average of y is given by similar equations. Inserting Eq. (10) into Eq. (3), we obtain the following hierarchy of equations for $\rho^{(j)}$:

$$\frac{\partial \rho^{(0)}}{\partial \tau} = 0, \tag{13}$$

$$\frac{\partial \rho^{(1)}}{\partial \tau} = D \frac{\partial^2 \rho^{(0)}}{\partial x^2} - \frac{\partial}{\partial x}[(Ax^3 + Bx^2 + Cx + Hy + I)\rho^{(0)}]$$

$$- \frac{\partial}{\partial y}[(Ex + Fy + G_0)\rho^{(0)}] - \frac{\partial \rho^{(0)}}{\partial t}, \tag{14}$$

$$\frac{\partial \rho^{(2)}}{\partial \tau} = D \frac{\partial^2 \rho^{(1)}}{\partial x^2} - \frac{\partial}{\partial x}[(Ax^3 + Bx^2 + Cx + Hy + I)\rho^{(1)}]$$

$$- \frac{\partial}{\partial y}[(Ex + Fy + G_0)\rho^{(1)}] - \frac{\partial \rho^{(1)}}{\partial t}$$

$$- Q \sin(\omega_p t)\frac{\partial \rho^{(0)}}{\partial y}, \tag{15}$$

where the normalization condition

$$\int_{-\infty}^{+\infty}\int_{-\infty}^{+\infty} \rho^{(n)}(x,y,t)dxdy = \delta_{0n} \tag{16}$$

follows from Eq. (4). Equation (13) implies that $\rho^{(0)}$ is independent of τ. Then, the terms in the right side of Eq. (14) which do not have τ-dependent coefficients give rise to secular terms (unbounded on the τ-time scale). The condition that no secular terms should appear is

$$D \frac{\partial^2 \rho^{(0)}}{\partial x^2} - \frac{\partial}{\partial x}[(Ax^3 + Bx^2 + Cx + Hy + I)\rho^{(0)}]$$

$$- \frac{\partial}{\partial y}[(Ex + Fy + G_0)\rho^{(0)}] - \frac{\partial \rho^{(0)}}{\partial t} = 0. \tag{17}$$

This equation should be solved for $\rho^{(0)}$ together with the normalization condition and the initial condition data. This is most easily done in Fourier space, in which the above equation reads

$$i\omega\hat{\rho}^{(0)} = D \frac{\partial^2 \hat{\rho}^{(0)}}{\partial x^2} - \frac{\partial}{\partial x}[(Ax^3 + Bx^2 + Cx + Hy + I)\hat{\rho}^{(0)}]$$

$$- \frac{\partial}{\partial y}[(Ex + Fy + G_0)\hat{\rho}^{(0)}]. \tag{18}$$

Note that this problem is equivalent to solving the FPE (3) without the probe signal as the effects of the probe signal appear first when calculating the first-order correction, $\rho^{(1)}$.

To calculate these first-order corrections, we again impose the condition that no secular terms appear, and that the right-hand side of Eq. (15) vanishes. The resulting equation is

$$D \frac{\partial^2 \rho^{(1)}}{\partial x^2} - \frac{\partial}{\partial x}[(Ax^3 + Bx^2 + Cx + Hy + I)\rho^{(1)}] - \frac{\partial}{\partial y}$$

$$\times[(Ex + Fy + G_0)\rho^{(1)}] - \frac{\partial \rho^{(1)}}{\partial t} - Q \sin(\omega_p t)\frac{\partial \rho^{(0)}}{\partial y} = 0. \tag{19}$$

In Fourier space we obtain,

$$i\omega\hat{\rho}^{(1)} = D \frac{\partial^2 \hat{\rho}^{(1)}}{\partial x^2} - \frac{\partial}{\partial x}[(Ax^3 + Bx^2 + Cx + Hy + I)\hat{\rho}^{(1)}]$$

$$- \frac{\partial}{\partial y}[(Ex + Fy + G_0)\hat{\rho}^{(1)}] - i\frac{Q}{2}\frac{\partial}{\partial y}$$

$$\times[\hat{\rho}^{(0)}(\omega + \omega_p) - \hat{\rho}^{(0)}(\omega - \omega_p)], \tag{20}$$

where

$$\hat{\rho}^{(j)}(x,y,\omega) = \int_{-\infty}^{\infty} dt e^{-i\omega t}\rho^{(j)}(x,y,t), \tag{21}$$

$$\langle \hat{x} \rangle^{(j)} = \int_{-\infty}^{+\infty}\int_{-\infty}^{+\infty} dxdy\, x\hat{\rho}^{(j)}(x,y,t), \tag{22}$$

$$j = 0,1. \tag{23}$$

Equation (20) should be solved for $\hat{\rho}^{(1)}$ together with $\int_{-\infty}^{+\infty}\int_{-\infty}^{+\infty} dxdy\hat{\rho}^{(1)} = 0$. Since $\rho^{(0)}$ evolves to a stationary solution for long time [i.e., $\hat{\rho}^{(0)} = \delta(\omega)f(\delta_1, \delta_2)$], we find that $\hat{\rho}^{(1)} = 0$ is the only solution of Eq. (20), unless $\omega = \pm \omega_p$. Then Eqs. (20) and (23) imply that

$$\hat{\rho}^{(1)} = \eta^+(x,y)\delta(\omega - \omega_p) + \eta^-(x,y)\delta(\omega + \omega_p). \tag{24}$$

Inserting Eq. (24) in Eq. (20), we obtain two uncoupled equations for η^+ and η^-. These can be solved, by expanding $\eta^{\pm}$ in Hermite polynomials,

$$\eta^{\pm}(x,y) = \sum_{n=0}^{\infty}\sum_{m=0}^{\infty}(T^{\pm})_n^m H_n(x)H_m(y)e^{-x^2}e^{-y^2}, \tag{25}$$

and solving the corresponding nonlinear systems of equations for the coefficients $(T^{\pm})_n^m$. Once we obtain $(T^{\pm})_n^m$, we can calculate $\langle \hat{x} \rangle^{(1)}$ from Eq. (23). Note that $\hat{\rho}(+\omega_p) = \hat{\rho}^*(-\omega_p)$, by taking the complex conjugate in Eqs. (20) and (23). Then it follows from Eqs. (24) and (25) that $(T^+)_n^m = ((T^-)_{-n}^{-m})^*$. Therefore we conclude that $\langle \hat{x} \rangle^{(1)}(-\omega_p) = [\langle \hat{x} \rangle^{(1)}]^*(+\omega_p)$, and the inverse Fourier transform yields

$$\langle x \rangle^{(1)}(t) = 2 \operatorname{Re}(\langle \hat{x} \rangle^{(1)}(\omega_p))\cos(\omega_p t)$$

$$- 2 \operatorname{Im}(\langle \hat{x} \rangle^{(1)}(\omega_p))\sin(\omega_p t). \tag{26}$$

Knowing $\langle x \rangle^{(1)}(t)$, the amplitude can be readily computed

$$A_{\langle x \rangle} = 2\sqrt{\langle \hat{x} \rangle^{(1)}(\langle \hat{x} \rangle^{(1)})^*} + O(\epsilon^2). \tag{27}$$
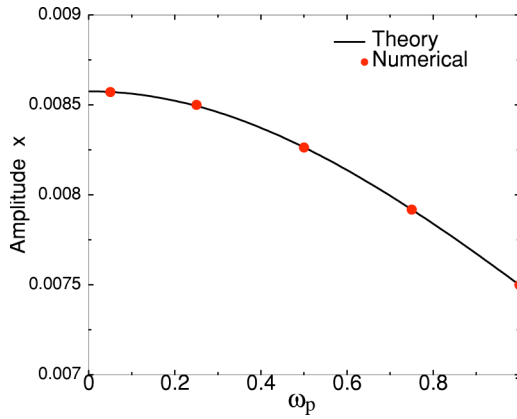
FIG. 4. Comparison between the theoretical results and the numerical simulations, marked by symbols. Parameters are $D=20$, $b_0=0.3$, $p=1$, $q=0.01$, $\alpha=0.05$, and $a=0.5$.

The advantage of the above procedure is that it only requires solving stationary equations. Rather than having to calculate a fully time-dependent solution and waiting until transients have disappeared, the amplitude of the oscillations can be found by solving the stationary problem Eq. (18) for $\hat{\rho}^{(0)}$, followed by solving a stationary problem for $\hat{\rho}^{(1)}$. To verify that the expansion in ε can be safely truncated at first order, we have plotted in Fig. 4 the amplitude of $\bar{x}$ using the full FPE equation (3) (solid circles) and using the theoretical approximation (27) (solid line). The agreement is remarkable, although it should be noted that the amplitude of the probe signal considered here is small ($q=0.01$).

For increasing strength of the probing amplitude, higher orders in the expansion may be required. However, once $\rho^{(1)}$ is known, it is also straightforward to find the successive terms in the expansion. Without entering into a detailed study, some general features can easily be drawn from the hierarchy of equations for $\rho^{(j)}$. Similarly to the analysis for $\hat{\rho}^{(1)}$, and by taking into account that $\hat{\rho}^{(1)}$ is a function exclusively of $\omega \pm \omega_p$, it is straightforward to prove that $\hat{\rho}^{(2)}=0$ is the only solution, unless $\omega=0, \pm 2\omega_p$. In general, successive terms will depend on higher harmonics of the main frequency ω_p.

FIG. 6. Maximum of $A_{\langle x \rangle}$ vs the noise strength D for three different number of coefficients. The results are obtained using Eq. (27) with parameters set as in Fig. 5, with $b_0=0.5$.

In Figs. 5(a) and 5(b) we apply the theory to parameter sets for which the deterministic system is excitatory (i.e., exhibits a stable fixed point), respectively, oscillatory. In both cases, as the figures demonstrate, decreasing the noise level leads to the appearance of a clear maximum for a nonzero value of ω_p. For the parameters of Fig. 5(b) this is not surprising, since for zero noise levels the system is oscillatory (with $A_{\langle x \rangle}=1.03$ and $\omega=0.24$). For the excitatory case [Fig. 5(a)] and in the absence of a probe signal, nonzero noise levels can lead to occasional escapes from the fixed point, leading to an underlying frequency. The inclusion of the probe signal will then result in a classical resonance when the probe signal frequency matches this underlying frequency [10,11].

Using the expression for $A_{\langle x \rangle}$ we can determine the location of the maximum. In Fig. 6, we plot the maximum in $A_{\langle x \rangle}$, which corresponds to the underlying frequency, as a function of the noise strength D, for different numbers of coefficients. As expected, for small values of noise the number of coefficients should be increased to achieve higher accuracy. Note that there exists a critical value of the noise below which the underlying frequency is different from zero.
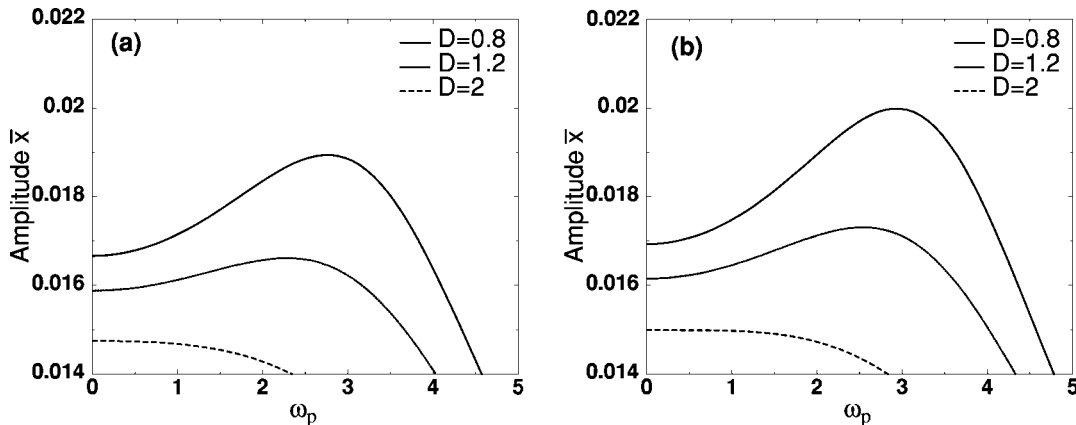

FIG. 5. Amplitude of $\bar{x}$ as a function of the frequency of the probe signal for different values of the noise strength. The amplitude was calculated using Eq. (27). The parameters are $p=1$, $q=0.01$, $\alpha=0.05$, and $a=0.5$. b_0 was chosen such that the noiseless system is excitatory in (a), where $b_0=0.2$, and oscillatory in (b), where $b_0=0.5$ and where the noiseless system has a frequency of $\omega \sim 4.1$.
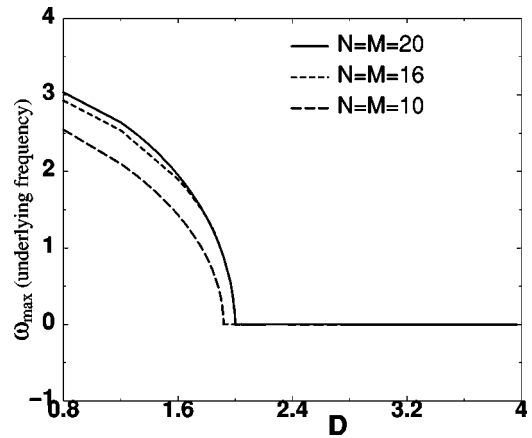
This is in full agreement with results plotted in Fig. 3 via Langevin simulations. In addition, notice that the dependence of the underlying frequency is well described by a square-root dependence on the noise strength, a familiar result for supercritical bifurcations.

III. GLOBALLY COUPLED SYSTEM

A. The FPE

We now extend the model equations (1) to include a global coupling term; this coupling scheme is the most amenable to theoretical treatment. The resulting Langevin equations are

$$\frac{dx_i}{dt} = Ax_i^3 + Bx_i^2 + Cx_i + Hy_i + I + \frac{K}{N}\sum_{j=1}^{N}(x_j - x_i) + \xi_i,$$

$$\tag{28}$$

$$\frac{dy_i}{dt} = Ex_i + Fy_i + G, \quad i = 1,\ldots,N. \tag{29}$$

Note that for a perfectly synchronized system this form of coupling reduces to the previously discussed single-element equation.

We are interested in an analytical investigation of the dynamics for very large N. In the thermodynamic limit, $N \to \infty$, it is well known [25] that models with mean-field coupling are described by an evolution equation for the one-particle probability density. This can be seen by noting that the hierarchy of equations for all the multiparticle probability densities can be closed by assuming molecular chaos, which states that there are no correlations among the oscillators. Hence, the one-system probability density $\rho(x,y,t)$ is asymptotically (i.e., in the limit, $N \to \infty$) the solution of the following nonlinear Fokker-Planck equation:

$$\frac{\partial \rho}{\partial t} = D\frac{\partial^2 \rho}{\partial x^2} - \frac{\partial}{\partial x}[(Ax^3 + Bx^2 + Cx + Hy + K(\bar{x}-x) + I)\rho]$$

$$-\frac{\partial}{\partial y}[(Ex + Fy + G)\rho], \tag{30}$$

where

$$\bar{x} = \int_{-\infty}^{+\infty}\int_{-\infty}^{+\infty} dx\, dy\, x\rho(x,y,t). \tag{31}$$

Analogous to the case of the single element, we will solve the FPE using an expansion in Hermite polynomials. The hierarchy (6) now becomes a system of coupled first-order nonlinear differential equations
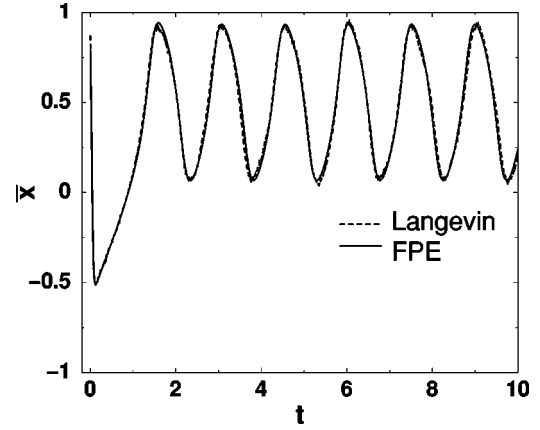

FIG. 7. Comparison between solution obtained by means of FPE, and direct numerical simulation of the Langevin equations for 5000 oscillators. Parameters are $b=0.5$, $p=1$, $\alpha=0.05$, $a=0.5$, $D=4$, and $K=10$.

$$\dot{r}_n^m = \left(\frac{3}{2}An^2 + Cn + Fm - Kn\right)r_n^m + [B(n-1)+I$$

$$+\pi K r_1^0]r_{n-1}^m + \left[D + \frac{3}{4}A(n-1) + \tfrac{1}{2}C - \frac{K}{2}\right]r_{n-2}^m$$

$$+\frac{B}{4}r_{n-3}^m + \frac{A}{8}r_{n-4}^m + Bn(n+1)r_{n+1}^m$$

$$+An(n+1)(n+2)r_{n+2}^m + Gr_n^{m-1} + \frac{F}{2}r_n^{m-2}$$

$$+\frac{1}{2}(H+E)r_{n-1}^{m-1} + E(n+1)r_{n+1}^{m-1} + H(m+1)r_{n-1}^{m+1},$$

$$\text{where} \quad n = 0,\ldots,\infty, m = 0,\ldots,\infty, \tag{32}$$

Again, to compare our FPE to direct numerical simulations we will truncate the above infinite hierarchy. A comparison between this truncation and the solution of the Langevin equations for a large number of FHN oscillators (5000) is shown in Fig. 7. The solution of the FPE, corresponding to $N \to \infty$, provides excellent agreement with the finite N case and shows that 5000 is already close to infinity for all practical purposes. As an aside, we mention here that for the coupled system the advantage of using the FPE becomes very clear. The numerical computation of the FPE was approximately 80 times faster than the direct Langevin calculation.

B. Bifurcation for the coupled system

The above example illustrates that, in contrast to the single-element case, where the FPE has a unique stationary solution, the FPE for the coupled system can exhibit time-dependent solutions. In fact, by varying the parameters, the system can undergo a stochastic Hopf bifurcation. This is shown in Fig. 8 for two different values of the coupling strength. In Fig. 9(a) we have plotted the amplitude of $\bar{x}$ as a function of the coupling strength K for a fixed level of noise,
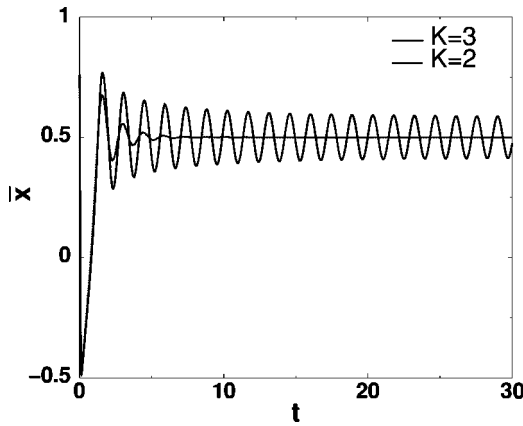
FIG. 8. The amplitude of $\bar{x}$ as a function of time for two different values of the coupling showing a clear bifurcation. Other parameters are as in Fig. 7.

FIG. 10. Amplitude of $\bar{x}$ vs the frequency of the probe signal for three different values of the coupling strength. Parameters are as in Fig. 7.

and for two different values of b. For these values of b, the deterministic system is synchronized and oscillatory. Below some critical coupling strength, the noise destroys the synchronization and $\bar{x}$ is no longer oscillatory. Consequently, the solution of the FPE is stationary. Upon increasing the coupling strength past this critical value, the system synchronizes and exhibits a time-dependent behavior. As in Fig. 6, the bifurcation is well described by a square-root dependence on the order parameter. The Hopf bifurcation is further illustrated in Fig. 9(b), where we have plotted the amplitude of $\bar{x}$ as a function of the noise strength for a fixed coupling strength. Again, the system displays a Hopf bifurcation which correspond to a transition from unsynchronized to synchronized dynamics: below the critical noise level, the solution is time dependent and the elements are synchronized while above the critical noise level, the solution is stationary and the elements are unsynchronized.

The behavior of the noisy globally coupled system is more complicated for parameter values for which the deterministic system is excitatory. Possible dynamics include noise-induced synchronization [26] and system size coherence resonance [27,18]. A systematic investigation of this regime will be the topic of a future publication.
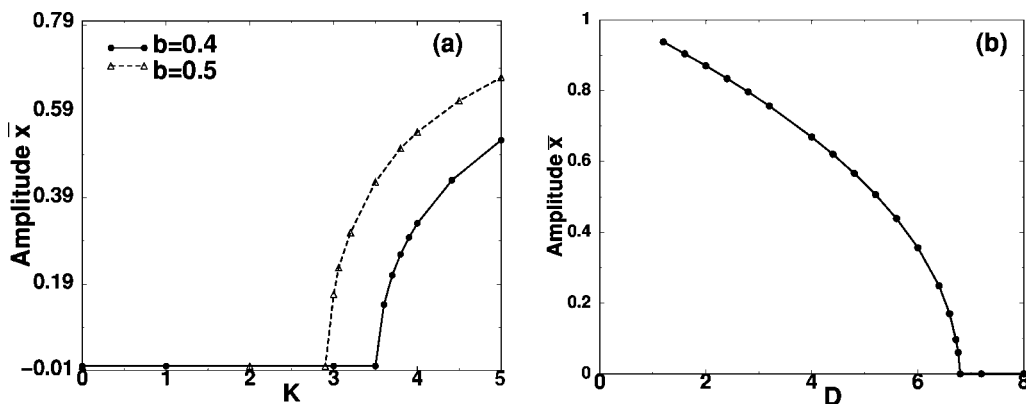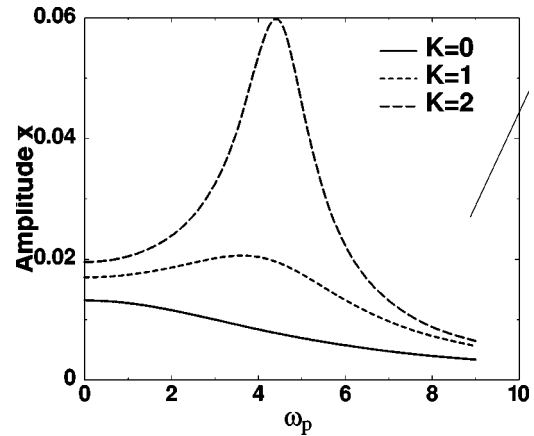
The inclusion of a probe signal will elicit a time-dependent solution of the FPE, even when the system *without* the probe signal has a stationary solution. As in the single-element case, the amplitude $\bar{x}$ of the response depends critically on the frequency of the probe signal as is shown in Fig. 10. For $K=0$ the response curve does not exhibit a peak showing that there is no underlying frequency in the problem. Increasing K produces an underlying frequency which appears as a peak in the curve. Note that for $K>2.9$ the system will synchronize in the absence of a probe signal (peak at $\omega_p=0$). This, then, leads to a response that has two principal frequencies: the frequency arising from the Hopf bifurcation and the probe frequency. Note also that in contrast to similar coupled systems (see, e.g., Ref. [11]), increasing the coupling does not lead to the ''death'' of the oscillatory region.

IV. CONCLUSIONS

In this paper, we have investigated the noisy single and globally coupled FHN model subject to an external time-sinusoidal injection (or ''probe'') signal. We have derived a FPE for the system and shown that we can solve this FPE

FIG. 9. (a) Amplitude of $\bar{x}$ as a function of the coupling strength for a fixed level of noise and two different values of b. (b) Amplitude of $\bar{x}$ as a function of noise, kept fixed $K=5$. Other parameters are as in Fig. 7.

efficiently by using a suitably chosen expansion. We find that there is a classical (or deterministic) resonance effect when the frequency of the probe signal approaches the underlying system frequency. We were able to characterize this resonance by separating the fast and slow time scales in the problem and find that, for small driving amplitudes, the agreement between numerical and analytical results is excellent. Our work was motivated by our earlier investigations [11] into the saddle-node bifurcation that underpins the dynamics of a dc SQUID; in that work, we showed that the system performed optimally (in the presence of a noise floor) when it was tuned so that the frequency of an external "target" signal (that was the subject of our detection procedure) was coincident with the internal frequency; an *a priori* knowledge of the internal frequency, in terms of deterministic system control parameters could then permit us to determine the target frequency by adjusting the SQUID parameters until the resonance depicted in Figs. 5 or 10, was realized. There are important differences in the dynamics, of course: the FHN system undergoes a Hopf bifurcation, and the natural frequency does not decrease with the number of coupled elements. A side product of our current work, is the characterization of the bifurcation behavior in the coupled system, in the presence of noise, without the necessity of truncating a moment system derived from the Langevin dynamics; we have shown that such a truncation can lead to misleading results.

Future work will include the further investigation of the response of the globally coupled system to the probe signal. In particular, parameter values for which the deterministic system is excitatory will be explored. Also, attention will be paid to the possibility that, upon inclusion of an input signal, a population can become synchronized and can produce a large output signal. By varying the intrinsic parameters, including the coupling constant, the response can thus be "tuned" at different frequencies.

[1] For reviews see A.R. Bulsara and L. Gammaitoni, Phys. Today **49**(3), 39 (1996); L. Gammaitoni, P. Hänggi, P. Jung, and F. Marchesoni, Rev. Mod. Phys. **70**, 223 (1998).

[2] See, e.g., J. Lindner, S. Chandramouli, A. Bulsara, M. Locher, and W. Ditto, Phys. Rev. Lett. **23**, 5048 (1998), and references therein.

[3] L. Arnold, *Random Dynamical Systems* (Springer Verlag, Berlin, 1999).

[4] M. Inchiosa and A. Bulsara Phys. Rev. E **53**, R2021 (1996); C. Heneghan, C.C. Chow, J.J. Collins, T.T. Imhoff, S.B. Lowen, and M.C. Teich, *ibid.* **54**, R2228 (1996); F. Chapeau-Blondeau, *ibid.* **55**, 2016 (1997); J. Robinson, D. Asraf, A. Bulsara, and M. Inchiosa, Phys. Rev. Lett. **81**, 2850 (1998); M. Inchiosa, J. Robinson, and A. Bulsara, *ibid.* **85**, 3369 (2000); S. Kay, IEEE Signal Process. Lett. **7**, 8 (2000); I. Goychuk and P. Hänggi, Phys. Rev. E **61**, 4272 (2000); J. Robinson, J. Rung, A. Bulsara, and M. Inchiosa, *ibid.* **63**, 011107 (2001).

[5] For reviews see M. Locher *et al.*, Chaos **8**, 604 (1998); R. Albert and A. Barabasi, Rev. Mod. Phys. **74**, 47 (2002).

[6] R. Fitzhugh, Biophys. J. **1**, 445 (1961).

[7] J. Nagumo, S. Arimoto, and S. Yoshizawa, Proc. IRE **50**, 2061 (1962).

[8] C. Koch, *Biophysics of Computation: Information Processing in Single Neurons* (Oxford, New York, 1999).

[9] *Theory of Heart*, edited by L. Glass, P. Hunter, and A. McCulloch (Springer Verlag, Berlin, 1991).

[10] S. Massanes and C. Vicente, Int. J. Bifurcation Chaos Appl. Sci. Eng. **9**, 2295 (1999).

[11] K. Wiesenfeld, A. Bulsara, and M. Inchiosa, Phys. Rev. B **62**, R9232 (2000); M. Inchiosa, V. In, A. Bulsara, K. Wiesenfeld, T. Heath, and M. Choi, Phys. Rev. E **63**, 066114 (2001); J. Acebron, W.-J. Rappel, and A. Bulsara, *ibid.* **67**, 016210 (2003); J. Acebron, A. Bulsara, and W.-J. Rappel, Fluct. Noise Lett. (to be published).

[12] A. Hodgkin and A. Huxley, J. Physiol. (London) **117**, 500 (1952).

[13] J. P. Keener and J. Sneyd, *Mathematical Physiology* (Springer Verlag, Berlin, 1998).

[14] A. Winfree, Chaos **1**, 303 (1991); A. Hagberg and E. Meron, Nonlinearity **7**, 805 (1994).

[15] C. Schurrer and K. Schulten, Physica D **50**, 311 (1991); A. Longtin, J. Stat. Phys. **70**, 309 (1993).

[16] H. Tuckwell and R. Rodriguez, J. Comput. Neurosci. **5**, 91 (1998).

[17] S. Tanabe and K. Pakdaman, Phys. Rev. E **63**, 031911 (2001).

[18] R. Toral, C. Mirasso, and J. Gunton, Europhys. Lett. **61**, 162 (2003).

[19] A. Longtin, Chaos, Solitons Fractals **11**, 1835 (2000); B. Lindner and L. Schimansky-Geier, Phys. Rev. E **60**, 7270 (1999); A. Pikovsky and J. Kurths, Phys. Rev. Lett. **78**, 775 (1997); C. Kurrer and K. Schulten, Phys. Rev. E **51**, 6213 (1995).

[20] H. Risken, *The Fokker Planck Equation* (Springer Verlag, Berlin, 1996).

[21] A. Zorzano, H. Mais, and L. Vasquez, Appl. Math. Comput. **98**, 109 (1999).

[22] M. Kostur, X. Sailer, and L. Schimansky-Geier, Fluct. Noise Lett. **3**, L155 (2003).

[23] J. Acebron, A. Bulsara, M. Inchiosa, and W.-J. Rappel, Europhys. Lett. **56**, 354 (2001).

[24] K. Schenk-Hoppé, Int. J. Non-Linear Mech. **31**, 685 (1996).

[25] R. Desai and R. Zwanzig, J. Stat. Phys. **19**, 1 (1978); M. Shiino, Phys. Lett. **112A**, 302 (1985); Phys. Rev. A **36**, 2393 (1987).

[26] W.-J. Rappel and A. Karma, Phys. Rev. Lett. **77**, 3256 (1996).

[27] A. Pikovsky, A. Zaikin, and M. de la Casa, Phys. Rev. Lett. **88**, 050601 (2002).